Molecular Biology of the Cell
Vol. 14, 4140–4154, October 2003

Maximal Polar Growth Potential Depends on the Polarisome Component AgSpa2 in the Filamentous Fungus *Ashbya gossypii*

Philipp Knechtle,* Fred Dietrich,† and Peter Philippsen‡§

Applied Microbiology, Biozentrum, Universitaet Basel, 4056 Basel, Switzerland

Submitted March 22, 2003; Revised June 17, 2003; Accepted June 17, 2003
Monitoring Editor: David Drubin

We used actin staining and videomicroscopy to analyze the development from a spore to a young mycelium in the filamentous ascomycete *Ashbya gossypii*. The development starts with an initial isotropic growth phase followed by the emergence of germ tubes. The initial tip growth speed of 6–10 μm/h increases during early stages of development. This increase is transiently interrupted in response to the establishment of lateral branches or septa. The hyphal tip growth speed finally reaches a maximum of up to 200 μm/h, and the tips of these mature hyphae have the ability to split into two equally fast-growing hyphae. A search for *A. gossypii* homologs of polarisome components of the yeast *Saccharomyces cerevisiae* revealed a remarkable size difference between Spa2p of both organisms, with AgSpa2p being double as long as ScSpa2p due to an extended internal domain. AgSpa2 colocalizes with sites of polarized actin. Using time-lapse videomicroscopy, we show that AgSpa2p-GFP polarization is established at sites of branch initiation and then permanently maintained at hyphal tips. Polarization at sites of septation is transient. During apical branching the existing AgSpa2p-GFP polarization is symmetrically divided. To investigate the function of AgSpa2p, we generated two AgSPA2 mutants, a partial deletion of the internal domain alone, and a complete deletion. The mutations had an impact on the maximal hyphal tip growth speed, on the hyphal diameter, and on the branching pattern. We suggest that AgSpa2p is required for the determination of the area of growth at the hyphal tip and that the extended internal domain plays an important role in this process.

INTRODUCTION

The ability of cells to polarize is essential in the overall process of cellular morphogenesis (Drubin and Nelson, 1996). It allows the cell to establish and maintain spatially restricted components that mediate functions as diverse as vectorial transport in epithelial cells, directed cell movements in amoeba or leukocytes, and cell shape development during early embryogenesis, neurite outgrowth, or sustained polar growth of filamentous fungi (Weiner, 2002). A variety of studies from all of these systems demonstrate that small GTPases (Rac, Ras, and Rho) together with guanosine nucleotide exchange factors and GTPase-activating proteins are key players in establishment and maintenance of cell polarity and that the actin cytoskeleton provides the structural basis for polarization (Hall, 1998; Johnson, 1999; Pruyne and Bretscher, 2000a,b).

Morphogenesis in filamentous fungi, which leads to a branched mycelium, is most likely regulated by networks controlling polarization at different levels. During the development from a spore to a mycelium, cell polarity is established at first during germination of a spore. Polarized growth is directed to the periphery of the germ bubble to initiate germ tubes. Apical extension at the tips of germ tubes lead to the formation of hyphae. New sites of cell polarity are selected at the cortex of hyphae to initiate lateral branches. Septation, the incomplete cytokinesis in filamentous fungi that lack cell separation, also represents a polarization event, which occurs transiently to form hyphal compartments. Apical branching, also called tip branching, was so far only observed in few filamentous fungi and occurs when the apex of a polarized tip divides symmetrically to produce two growing tips. Another unique feature of filamentous fungi is their ability to accelerate hyphal tip extensions during development of the mycelium, and the so far not understood coordination between hyphal tip extension and hyphal branching. Together, the spatial and temporal organization of the different polarization events is crucial for optimal mycelial morphogenesis (Heath, 1995; Harris, 1997; Momany and Hamer, 1997; Lengeler *et al*., 2000; Momany and Taylor, 2000; Wendland, 2001; Momany, 2002; Ayad-Durieux *et al*., 2000; Trinci *et al*., 1994).

On a molecular level, the impact of polarized growth on hyphal morphogenesis has only recently begun to be investigated. In *Aspergillus nidulans*, it was shown that the formin homolog SEPA participates in septum formation and polarized growth (Harris *et al*., 1997, 1999; Sharpless and Harris, 2002), and the "swo" and "pod" mutants were associated with defects in hyphal polarity (Harris *et al*., 1999; Momany *et al*., 1999; Momany, 2002). In *Penicillium marneffei*, a CDC42 homolog was shown to be required for correct cell polarization (Boyce *et al*., 2001). Deletion of a CDC42 homolog in

Article published online ahead of print. Mol. Biol. Cell 10.1091/mbc.E03–03–0167. Article and publication date are available at www.molbiolcell.org/cgi/doi/10.1091/mbc.E03–03–0167.

Online version of this article contains video material for some figures. Online version is available at www.molbiolcell.org.

Present addresses: †Unité Biologie et Pathogénicité fongiques, Institut Pasteur, 25-28, Rue du Docteur Roux, 75724 Paris Cedex 15, France; ‡Duke Center for Genome Technology, Duke University Medical Center, Box 3568, Durham, NC 27710-3568.

§ Corresponding author. E-mail address: peter.philippsen@unibas.ch.

Ashbya gossypii or its putative guanosine nucleotide exchange factor still allowed isotropic growth of the spore but prevented the establishment of cell polarity (Wendland and Philippsen, 2001). In the same publication, AgRho3p was identified as important for polarity maintenance because, in the absence of this protein, hyphal tips frequently switched to isotropic growth and then reverted to polar growth in the previous axis of polarity. The function of the rhoGAP AgBem2p in *A. gossypii* was associated with the determination of cell polarity in germinated spores and hyphal tips (Wendland and Philippsen, 2000) and the PAK kinase AgCla4p, a potential effector of AgCdc42p, was shown to be required for hyphal maturation (Ayad-Durieux *et al*., 2000). Thus, conserved proteins that have been implicated in cell polarity in a variety of other organisms contribute to morphogenesis in filamentous fungi.

The spatial and temporal organization of polarization in a developing mycelium, specifically the coordination of different polarization events and the impact of polarization on the maximal speed potential of hyphal tips have so far been little or not investigated. We wanted to find candidate genes in the genome of the filamentous fungus *A. gossypii* implicated in the regulation of these processes to extend our investigations about polarity control. We hypothesized that orthologs of such genes should be either absent in *Saccharomyces cerevisiae* or substantially altered, e.g., coding for additional domains with no homology in *S. cerevisiae*. We favored *A. gossypii* for these studies because its genome is small and its sequence is largely known (Dietrich *et al*., 2001) and because molecular genetic techniques are well established (Steiner *et al*., 1995; Altmann-Johl and Philippsen, 1996; Wendland *et al*., 2000).

In *S. cerevisiae*, it has been shown that the actin cytoskeleton serves for the organization of growth and thus for morphogenesis (Lew and Reed, 1993). Secretory vesicles are transported along actin cables to sites of polarized growth (Finger and Novick, 1998) and the organization of the actin cable network includes components of the polarisome (Evangelista *et al*., 2002; Sagot *et al*., 2002). When we screened the *A. gossypii* genome, we found orthologs for all four polarisome components and with very similar domain composition except for ScSpa2. The ortholog AgSpa2p is more than twice as long as ScSpa2p and represents the sixth largest protein in *A. gossypii*.

A number of studies with *S. cerevisiae* have characterized ScSpa2p. It localizes to sites of polarized growth independent of actin. During the mitotic cycle, it is found at bud tips and at sites of cytokinesis and upon pheromone induction it localizes to sites of projection formation (Snyder, 1989; Gehrung and Snyder, 1990; Snyder *et al*., 1991). In cosedimentation experiments, Spa2p, Pea2p, and Bud6p form a large 12S multiprotein complex termed polarisome. Deletion phenotypes of strains lacking either ScSPA2 or the other polarisome components, ScPEA2 or ScBUD6, are very similar; cells are rounder than wild type, defective in mating projection formation, and specific for diploid cells, defective in bud site selection (Gehrung and Snyder, 1990; Sheu *et al*., 1998). ScSpa2p and ScBud6p both interact with the formin ScBni1p (Evangelista *et al*., 1997; Fujiwara *et al*., 1998), ScBud6p binds actin (Amberg *et al*., 1997), and ScPea2p is important for ScSpa2p stability and localization (Valtz and Herskowitz, 1996). Recently, it has been shown that ScBni1p directs actin filament assembly to sites of polarization where ScSpa2p mediates its localization and ScBud6p its activation (Evangelista *et al*., 2002; Sagot *et al*., 2002). Importantly, ScSpa2p also interacts with members of the mitogen-activated protein kinase cascades (Sheu *et al*., 1998; van Drogen and Peter, 2002).

Table 1. Plasmids and bacterial artificial chromosomes

Name	Reference
pGEN3	Wendland *et al.*, 2000
opAG13790	Dietrich *et al.*, 2001
pAGSPA2	This study
pAGSPA2ΔP	This study
pAGSPA2ΔP_TURA	This study
pFA6a_GFPS65T_kanMX	Wach *et al.*, 1997
pGUG	This study
pAGSPA2-GFP	This study
pUC19	Yanisch-Perron *et al.*, 1985
pBSIISK(+)	Short *et al.*, 1988
pTCAGSPA2-GFP	This study

In this article, we first document the spatial organization of the actin cytoskeleton at different developmental stages of *A. gossypii* and the localization of AgSpa2p-GFP to sites of polarized actin. Using time-lapse videomicroscopy, we show that AgSpa2p is part of an organelle that permanently localizes at hyphal tips, accumulates at cortical sites before lateral branch emergence, symmetrically splits during tip branching, and transiently localizes at sites of septation. We further examine phenotypes of total and partial deletions, in particular effects on hyphal maturation and branching, and we present evidence that AgSpa2p affects the area of growth at the hyphal tip, which subsequently has an impact on the hyphal tip growth speed and on the branching pattern.

MATERIALS AND METHODS

Molecular Cloning, Strains, Media, and Bioinformatics

Molecular cloning was done according to Sambrook *et al*., 2001. *Escherichia coli* DH5α (Hanahan, 1983) served as a host strain for all plasmid work. Plasmids and bacterial artificial chromosomes used in this work are listed in Table 1. DNA-modifying enzymes were purchased from New England Biolabs (Beverly, MA), *Taq*DNA polymerase was from Amersham Biosciences (Amersham Biosciences UK, Little Chalfont, Buckinghamshire, United Kingdom), and Pwo polymerase was from F. Hoffmann-La Roche (Basel, Switzerland). *A. gossypii* media preparation, culture conditions, and transformation protocols were perform as described in Wendland *et al*., 2000. *A. gossypii* strains are listed in Table 2. Media for *S. cerevisiae* were prepared as described in Guthrie and Fink, 1991. The transformation procedure was based on a protocol by Schiestl and Gietz, 1989. *S. cerevisiae* strains are listed in Table 3. Bioinformatic tools for alignment, database searching, protein analysis, primer selection, and pattern recognition were used from the Wisconsin Package (Genetics Computer Group, Cambridge, United Kingdom). ProfileScans were performed at the ISREC ProfileScan server http://hits.isb-sib.ch/cgi-bin/PFSCAN.

Cloning of pAGSPA2 and pAGSPA2ΔP

From a complete genome sequencing approach (Dietrich *et al*., 2001), we could locate the AgSPA2 gene on an 11,915-base pair fragment flanked by *Xma*I and *Xba*I restriction sites. Genomic *A. gossypii* DNA was digested *Xma*I/*Xba*I, and the DNA was separated by agarose gel electrophoresis. Fragments between 10.0 and 12.0 kbp were eluted and ligated with *Xma*I/*Xba*I digested pRS415. Positive pAGSPA2 clones were identified by a radioactive colony hybridization. As a probe, we used a 591-base pair *Eco*RV fragment from opAG13790 covering a part in the N-terminal coding region of AgSPA2. To construct pAGSPA2ΔP, pAGSPA2 was digested with the restriction enzymes *Stu*I and BtrI and the linearized plasmid was religated, thus releasing a 6558-base pair region from the AgSPA2 open reading frame (ORF). The sequence of the 11,915-base pair *Xma*I/*Xba*I fragment bearing the AgSPA2 ORF, a tRNA-Thr, and the C-terminal coding region of an ORF with homology to the *S. cerevisiae* gene YLR312C was submitted to GenBank under accession number AF515458.

Table 2. *A gossyp*II strains

Name	Genotype	Reference
Agleu2Δthr4Δ*	leu2Δ, thr4Δ	Altmann-Johl and Phillippsen, 1996; C Mohr, unpublished data
Agspa2ΔC	Agspa2Δ::GEN3, leu2Δ, thr4Δ	This study
AgSPA2ΔP-GFP	SPA2Δ(978–3163)::GEN3, leu2Δ, thr4Δ	This study
AgSPA2-GFP	AgSPA2-GFP::GUG, leu2Δ, thr4Δ	This study
AgSPA2ΔP-GFP	SPA2Δ(978–3163)-GFP::GUG, leu2Δ, thr4Δ	This study

*Referred to as wild type.

Generation of AgSPA2ΔP and Agspa2ΔC Strains

We used a polymerase chain reaction (PCR)-based approach (Wendland *et al*., 2000) to construct the Agspa2ΔC gene deletion. The dominant drug resistance marker GEN3 was amplified in a preparative PCR reaction from the *E. coli* plasmid pGEN3 by using the oligonucleotides 5′-GTGACCGGCAACTCGCAGGACCGCTCGACATCCACTCGCGCACAGGCTAGGGATAACAGGGTAAT-3′ and 5′-CGCTTCACGTGGAAGTGGTCCTTCGGCAATAGATGGT CCGGCTGTAGGCATGCAAGCTTAGATCT-3′. The oligonucleotides carried 45-base pair extensions at their 3′ site with homology to the AgSPA2 locus. Ten micrograms of PCR product was transformed into Agleu2Δthr4Δ, deleting the complete coding region of the AgSPA2 gene between the start and the stop codon. Correct integration of the cassette was verified by analytical PCR by using the oligonucleotides 5′-GTCAAAGAAACCCACACCC-3′ and 5′-GGCGGGCTAGTATAAATGTATC-3′ in combination with the standard oligonucleotides for GEN3. Six independent homokariotic Agspa2ΔC transformants were obtained. All experiments were done on at least on two independent isolates.

The AgSPA2ΔP strain was generated via transformation of a cloned and linearized cassette. First, the *S. cerevisiae* URA3 terminator and the GEN3 module were amplified in a preparative PCR reaction from the *E. coli* plasmid pGUG (see below) with the oligonucleotides 5′-CTTAAGGAGGAAATAGAATACTTAAACTCCAAATTGGCGAAGTAGattataagtaaatgcatgtatac-3′ and 5′-CTCTCTGTGCTACGTGAAAAGAGCGAGCACTGTATTAGAGAAGTTAGGGACCTGGCACGGAGC-3′. The oligonucleotides carried 45-base pairs homology extensions to the 3′-coding region of the AgSPA2 ORF and 39 base pairs downstream to the AgSPA2 stop codon, respectively. The PCR product was cotransformed with pAGSPA2ΔP into yeast strain #259(pFS-28)-3 [Table 3; #259(pFS-28)-3 lacks the TEF2 locus, which might interfere with the *S. cerevisiae* TEF2 promoter and terminator regions controlling the kanR in the GEN3 module]. Recombination between the PCR cassette and pAGSPA2ΔP was verified by analytical PCR by using oligonucleotide pairs 5′-TGACCATTTCGCTGACAAAC-3′ and 5′-GGAGATCTATGCGTCCATCTTTACAGTCC-3′ for amplification of the 5′ site and 5′-GGCGGGCTAGTATAAATGTATC-3′ and 5′-CTCCAACTCGGCACTATTTTAC-3′ for amplification of the 3′ site. The new plasmid pAGSPA2ΔP_TURA was digested with the restriction enzyme *Eco*RV to release a 4444-base pair fragment that was cloned into the *Eco*RV site of pBSIISK(+) to generate pTCAgSPA2ΔP. This *Eco*RV fragment carries 1634-base pair homology to the AgSPA2 ORF at the 5′ site of the *Stu*I/BtrI deletion and remaining 686 base pairs between the *Stu*I/BtrI deletion and the stop codon. At the 3′ site, it carries 156-base pair homology to the endogenous AgSPA2 terminator region. pTCAgSPA2ΔP was amplified in *E. coli*, and 5 μg was digested with *Eco*RV and transformed into Agleu2Δthr4Δ. Verification was done on homokaryotic mycelia. The 5′ site was amplified with the oligonucleotides 5′-CATAAGTCATTTGCCAATAGC-3′ and 5′-TCGCAGACCGATACCAGGATC-3′ and the 3′ site by using 5′-CAGGGCTCTTATGATGAACTTCC-3′ and 5′-GGAGATCTATGCGTCCATCTTTACAGTCC-3′. The deleted region in AgSPA2ΔP could not be amplified with the oligonucleotides 5′-TCGAGTATTCCTACATGATGGC-3′ and 5′-GCATTCGATTCACGCCGCAG-3′, whereas this was possible in AgleuΔthr4Δ. Two independent transformants were obtained that were used on all experiments.

Table 3. *S. cerevisiae* strains

Name	Genotype	Reference
#259(pFS-28)3	lys2, his4, URA3, tel2Δ	Schirmaier and Philippsen, 1984

Generation of AgSPA2-GFP and AgSPA2ΔP-GFP Strains

We first constructed a universal module for PCR-based C-terminal green fluorescent protein (GFP) fusion in *A. gossypii* in analogy to the GFP reporter modules for PCR targeting in *S. cerevisiae* (Wach *et al*., 1997). The strategy in this method is the generation of a transformation cassette for C-terminal GFP fusion in a preparative PCR reaction. A module consisting of the coding region of the GFP, a terminator, and a resistance marker is amplified by PCR. The primers used for amplification carry 45-base pair extensions at their 3′ sites. If the extension of the 5′ amplification primer is designed with homology to the C-terminal coding region before the stop codon, homologous recombination between the PCR cassette and the genomic locus will result in an extension of the ORF with the coding region for the GFP. The extension of the 3′ amplification primer is designed with homology after the stop codon. The basis for our module was the pFA6a-GFP(S65T)-kanMX6 (Wach *et al*., 1997), which consisted of the GFP(S65T) coding region (Heim and Tsien, 1996), the *S. cerevisiae* ADH terminator, and the kanMX6 marker (Wach *et al*., 1994). We replaced the kanMX6 marker (which contains *A. gossypii* sequences) by the GEN3 marker (Wendland *et al*., 2000). GEN3 was amplified from pGEN3 by PCR with the oligonucleotides 5′-ATCAGATCTGGTGTATTTACC-3′ and 5′-AGCTTTGTTTAAACGATGAGGCCGTCTTTTGTTG-3′. The PCR product was digested with the restriction enzymes *Bgl*II and PmeI and ligated into the *Bgl*II/PmeI sites of pFA6a-GFP(S65T)-kanMX6. To optimize the annealing sites for amplification and to get rid of unwanted restriction sites at the beginning and at the end of the module, we inserted the two complementary oligonucleotides 5′-GGGGCCGGTGCAGGCGCTGGAGCTGGCGCCGGTGCTGGCGCA-3′ and 5′-TGCGCCAGCACCGGCGCCAGCTCCAGCGCCTGCACCGGCCCC-3′ encoding a 7 × Gly-Ala peptide into the restriction site *Sma*I. At the 3′ site, we replaced the 22-base pair restriction fragment *Sac*I/*Spe*I with the complementary oligonucleotides 5′-ccgtgccaggtccctggggaga-3′ and 5′-ctagtctccccagggacctggcacggagct-3′. Surprisingly, the *S. cerevisiae* ADH terminator in this module displayed ARS activity in *A. gossypii*. The transformed PCR cassettes circularized and were maintained under appropriate selection conditions. We thus replaced the ADH terminator by the *S. cerevisiae* URA3 terminator. Two hundred and thirty-four base pairs from position 116,980–117,213 on Yeast chromosome V (Dietrich *et al*., 1997) were amplified with the oligonucleotides 5′-GGCGCGCCATTATAAGTAAATGCATGTATAC-3′ and 5′-GGAGATCTATGCGTCCATCTTTACAGTCC-3′. The PCR product was digested with the restriction enzymes AscI and *Bgl*II and cloned into the AscI/*Bgl*II sites. PCR products amplified from the newly constructed module did not show ARS activity anymore. The annealing sites for amplification by PCR were 5′-GGTGCAGGCGCTGGAGCTG-3′ at the 5′ site and 5′-AGGGACCTGGCACGGAGC-3′ at the 3′ site. The optimal PCR conditions determined were 2′ initial denaturation at 94°C′, 1′ denaturation at 93°C, 1′ annealing at 60°C, 2′ 45″ elongation at 72°C, 30 cycles, 7′ final elongation at 72°C, Pwo polymerase in the supplied reaction buffer adjusted to 4 mM $MgSO_4$. The module was 2738 base pairs in length and the plasmid named pGUG [GFP(S65T)-URA3T-GEN3]. The sequence was submitted to GenBank under accession number AF515459. To obtain a C-terminal GFP fusion of the AgSPA2 ORF, pGUG was amplified with the oligonucleotides 5′-AGCCTTAAGGAGGAAATAGAATACTTAAACTCCAAATTGGCGAAGGGTGCAGGCGCTGGAGCTG-3′ and 5′-CTCTCTGTGCTACGTGAAAAGAGCGAGCACTGTATTAGAGAAGTTAGGGACCTGGCACGGAGC-3′. The 45-base pair 3′ extensions were homologous to the C-terminal coding region of the AgSPA2 ORF and 39 base pairs downstream of the AgSPA2 ORF, respectively. A direct transformation of the PCR product into *A. gossypii* did not yield transformants. Thus, an alternative way via *S. cerevisiae* was chosen. The PCR product was transformed together with the plasmid pAGSPA2 (see above) into the yeast strain #259(pFS-28)-3. The transformants were verified for correct recombination of the PCR product with the plasmid; the 5′ linkage with the oligonucleotides 5′-CGCACTAAAAGAACACGGCAAC-3′ and 5′-ATCACCTTCACCCTCTCCAC-3′ and the 3′ linkage with 5′-GGCGGGCTAGTATAAATGTATC-3′ and 5′-CTCCAACTCGGCACTATTTTAC-3′. A 3180-base pair

fragment from the constructed pAGSPA2-GFP was excised with the restriction enzyme *Sal*I and subcloned into pUC19, generating pTCAGSPA2-GFP. The fragment consists of the GUG module flanked by homologous regions to the AgSPA2 locus, 218 base pairs at its 5′ site and 224 base pairs at its 3′ site. pTCAGSPA2-GFP was amplified in *E. coli*. Five micrograms of DNA was digested with *Sal*I and transformed into the Agleu2Δthr4Δ strain. Homokaryotic isolates were verified by PCR for correct integration of the module with the same oligonucleotides used for verification of the recombination on the plasmid. Two AgSPA2-GFP transformants were obtained, both of which displayed the same localization pattern.

To generate an AgSPA2ΔP-GFP strain, pAGSPA2-GFP was digested *Stu*I/BtrI to release a 6558-base pair fragment generating pAGSPA2ΔP-GFP (see above). A 5214-base pair *Eco*RV fragment from this plasmid was cloned into the *Eco*RV restriction site of pBSIISK(+), creating pTCAgSPA2ΔP-GFP. The new plasmid harbored the GFP module fused to the partially deleted AgSPA2 ORF. The homology region before the *Stu*I/BtrI deletion was 1634 base pairs in length; the region between the *Stu*I/BtrI deletion and the GFP was 686 base pairs in length. At the 3′ site of the GUG module, 156 base pairs of homology are located to the endogenous AgSPA2 terminator region. pTCAgSPA2ΔP-GFP was amplified in *E. coli* and digested with *Eco*RV. Five micrograms of DNA was transformed into the Agleu2Δthr4Δ strain to obtain AgSPA2ΔP-GFP. Homokaryotic transformants were verified by PCR with the oligonucleotides used for the verification of the AgSPA2-GFP strain and the AgSPA2ΔP strain, respectively.

Cytoskeletal Staining

Visualization of the actin cytoskeleton was done using phalloidin coupled fluorophores (according to Amberg, 1998, modified). *A. gossypii* was cultured in Ashbya Full Medium (AFM) to the desired developmental stage. One milliliter of the culture was mixed with 100 μl of 37% formaldehyde and fixed for 10 min. Mycelia were centrifuged at 2000 × *g*, resuspended in phosphate-buffered saline (PBS) containing 4% formaldehyde, and incubated for 1 h. Mycelia were washed twice with PBST (PBS containing 0.03% Triton X-100) and resuspended in 100 μl of PBST. Ten microliters of rhodamine-phalloidin or Alexa 488-phalloidin (6.6 μM in MeOH; Molecular Probes, Eugene, OR) was added, and the mycelia were incubated for 1 h in the dark. Mycelia were washed 5 times in PBST and resuspended in 50 μl of mounting medium (50 mg of *p*-phenylenediamine in 5 ml of PBS, adjusted pH to 8.0 with 0.5 M Na_2CO_3 pH 9.0, and brought volume to 50 ml with glycerol).

Alternatively, cells were fixed with paraformaldehyde if the fluorescence of GFP should be maintained. One milliliter of a cell culture was fixed for 30 min with 1 ml of 4% paraformaldehyde (Sambrook *et al.*, 2001). Mycelia were washed twice with PBST and resuspended in mounting medium or stained for actin by using rhodamine-phalloidin according to the protocol above.

Microscopy

Microscope Setup. The microscopy unit used (as described in Hoepfner *et al.*, 2000, modified) consisted of an Axioplan 2 imaging microscope (Carl Zeiss, Feldbach, Switzerland) with the objectives Plan Neofluar 100 × Ph3 numerical aperture (N.A.) 1.3, Plan Neofluar 63 × Ph3 N.A.1.25, Plan Neofluar 40 × Ph3 N.A.1.3, and Plan Apochromat 63 × N.A. 1.4. It was equipped with a 75 W XBO illumination source controlled by a MAC2000 shutter and filter wheel system (Ludl Electronics, Hawthorne, NY). The camera was a TE/CCD-1000PB back-illuminated cooled charge-coupled device camera (Princeton Instruments, Trenton, NJ). The following filter sets for different fluorophores were used: #10 for Alexa 488 and #20 for rhodamine (Carl Zeiss), #41018 for GFP (Chroma Technology., Brattleboro, VT). GFP-rhodamine double stainings were acquired with the mentioned filter sets except that the HQ500LP emission filter from filter set #41018 was replaced by a BP505–530 (Carl Zeiss). The excitation intensity was controlled with different neutral density filters (Chroma Technology). The setup, including microscope, camera, and Ludl controller, was controlled by MetaMorph 4.1.7 software (Universal Imaging, Downingtown, PA).

Image Acquisition and Processing. The illumination time and light intensity for standard brightfield or fluorescence acquisitions was chosen to reach minimally 25% of the maximal measurable intensity. For multiple exposures of the same sample, bleaching of the sample had to be taken into account. The z-distance in stack acquisitions was set to maximal 0.4 μm. Brightfield and single plane fluorescent images were scaled using the "scaling" drop-in in MetaMorph. Stacks were deblurred with MetaMorph's "remove shading" drop-in, flattened by "stack arithmetic," and scaled as mentioned above. For three-dimensional (3D) reconstructions, stacks were first deblurred using AutoDeblur 7.0 (Universal Imaging) and reconstructed with MetaMorph's "3D reconstruction" drop-in. For time-lapse acquisition, spores were cultured on a slide with a cavity (time-lapse slide) that was filled with medium (AFM, for fluorescent acquisitions 0.25 × AFM in respect to peptone, yeast extract, and myo-inositol, 1× in respect to glucose). Spores were preincubated in a humid chamber without coverslip until they reached the required developmental stage. Then, a coverslip was acquired. An acquisition set consisted of a brightfield image with optional three fluorescent images. The acquisition frequency varied from 0.5 to 0.2 min^{-1}. The exposure time for the fluorescent images was reduced to 0.2–0.4 s at 10–25% excitation intensity. Fluorescent pictures sets were processed as mentioned above and overlaid using MetaMorph's "overlay" drop-in. The time-lapse picture series was exported from MetaMorph as 8-bit TIFF files, converted to PICT files by Adobe Photoshop 6.0 (Adobe Systems, Mountain View, CA) for Mac (Apple Computer, Cupertino, CA) and converted to a QuickTime Movie (Apple Computer) by Adobe Premiere 4.2.1 for Mac. For time-lapse acquisitions with a frequency of 0.5 h^{-1}, microscopy slides were covered with 1 ml of molten AFM agar. Spores were spread on slides and allowed to germinate in a humid chamber to prevent drying of the agar. The slides were only removed from the humid chamber to acquire pictures.

RESULTS

Actin Cytoskeleton in Developing *A. gossypii* Mycelium

As a first step to characterize polarization in *A. gossypii*, we visualized its actin cytoskeleton at different developmental stages. Spores were incubated in liquid AFM. Starting after 6 h, aliquots were taken every 2 h, fixed with formaldehyde, and stained with rhodamine-phalloidin. Typical developmental stages are shown in Figure 1 and Movie 1. Spores of *A. gossypii* are needle shaped, and isotropic growth during germination is restricted to the middle of the needle, the location of the haploid nucleus. During this phase actin patches localize randomly at the cortex of the germ bubble (Figure 1A). Accumulation of actin patches perpendicular to the axis of the needle marks the initiation of the first germ tube (Figure 1B) the growth of which resembles the formation of a yeast bud with polarized actin patches at the expanding surface and actin cables emerging from the growing tip (Figure 1C). Unlike in budding yeast, the first germ tube continues extending and an additional site at the cortex of the germ bubble polarizes actin to mark the initiation of the second germ tube opposite of the first germ tube. Furthermore, an actin ring at the junction of germ bubble and first germ tube initiates the formation of the first septum (Figure 1D). The two germ tubes continue to grow by tip extension, the typical growth mode of hyphae. During this continued hyphal extension lateral branches and septa are initiated, the first branch usually next to the first septum. One or two further germ tubes may initiate.

An example of this developmental stage, called young mycelium, is shown in Figure 1E. Three germ tubes and two lateral branches are seen that are actively growing, indicated by accumulation of actin patches in their tip regions. These growth zones seem to be connected by long actin cables like wires along the cortex of the young mycelium (3D reconstruction; Movie 1). Different developmental stages of septation are visible at the necks between germ tubes and germ bubble and adjacent to the second branch (Movie 1 and arrows in Figures 1, D and E, and 4 (right): Δ, neck before septation; r, actin ring, a prerequisite of septum formation; +, actin patches on both sides of a growing septum; and *, completed septum lacking actin). All germ tubes and lateral branches develop into fast-growing hyphae, which after ~20 h start dividing at their tips, a branching mode typical for mature *A. gossypii* mycelium (Figure 1F).

AgSpa2p Is a Conserved Protein with an Extended Internal Domain

AgSpa2p has homology to ScSpa2p (Snyder, 1989) and Sph1p (Arkowitz and Lowe, 1997) in *S. cerevisiae* and to CaSpa2p from *Candida albicans* (originally named IPF11245; http://genolist.pasteur.fr/CandidaDB/). AgSpa2p has a predicted length of 3392 aa, ScSpa2p and CaSpa2p are 1466 aa in length, and ScSph1p 648 aa. Figure 2A shows a ClustalW

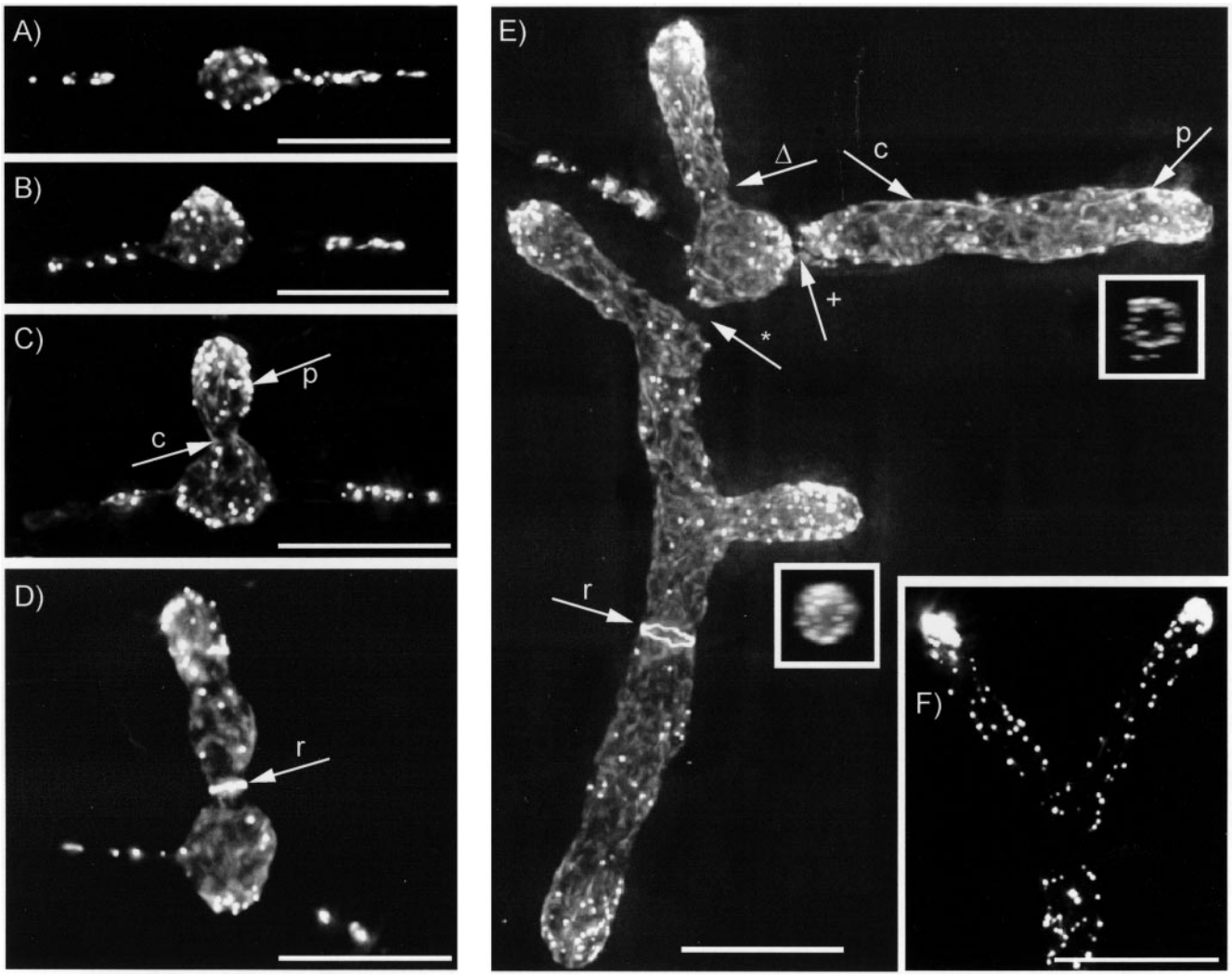

Figure 1. *A. gossypii* rhodamine-phalloidin stainings during development from a spore to a mature mycelium. See text for description. The rectangles in Figure 1E show a horizontal view on the top of the respective tips. The most apical part of the tip is free of actin patches and forms a "hole" (see also the animated 3D reconstruction in Movie 1). Fluorescence can also be observed in the needle-shaped spores. The origin and importance of these structures is elusive. Bar, 10 μm. p, actin patch; c, actin cable; Δ, neck before septation; r, actin ring, a prerequisite of septum formation; +, actin patches on both sides of a growing septum; and *, completed septum lacking actin.

analysis (Thompson *et al*., 1994) applied to identify conserved domains in these proteins. Four common domains could be identified in AgSpa2p, ScSpa2p, and CaSpa2p termed SHD Ia, Ib, II, and V (Roemer *et al*., 1998). Our analysis revealed that the originally annotated SHD I actually consists of two separate blocks of homology. Orthologs of known interactors with SHD Ia, II, and V in *S. cerevisiae* are present in *A. gossypii* (Figure 2, see legend). Regions with predicted coiled coils (Steinert and Roop, 1988) were located between SHD Ib and SHD II in AgSpa2p, Scspa2p, and CaSpa2p but were missing in ScSph1p. The increased length of the *A. gossypii* protein is due to an extended internal domain between SHD II and SHD V, which is about 3 times as large as in ScSpa2p or CaSpa2p and 10 times as large as in ScSph1p as concluded from DotPlot analysis (Maizel and Lenk, 1981; data not shown). No significant homology could be located in this internal domain comparing the three proteins to each other. AgSpa2p contains a highly repetitive region of ~800 aa in the internal domain (Figure 2B). The core of this repetitive region is a 10-aa repeat of the sequence SPA(R,L)G(E,D)(L,V)(I,K)S(T,V) repeated 30 times (with two substitutions allowed). Less conserved fragments of this repeat are spread all over the internal domain. A 9-aa repeat was previously identified in ScSpa2p in its internal domain (Snyder, 1989). Both repeats share only the initial Ser-Pro unit. The DNA sequence of AgSPA2 is also highly repetitive in the coding region for the AgSpa2p repeat (Figure 2B). Similar DNA repeats are not conserved in the ScSPA2 ORF. No repeated peptide sequence was observed in CaSpa2p nor in ScSph1p, but Ser-Pro units were also distributed in the respective internal domains. The AgSPA2 locus of *A. gossypii* displayed ancient synteny to the ScSPA2 and the ScSPH1 loci in *S. cerevisiae*, proving that ScSPA2 and ScSPH1 originated from one ancestral gene (Figure 2C).

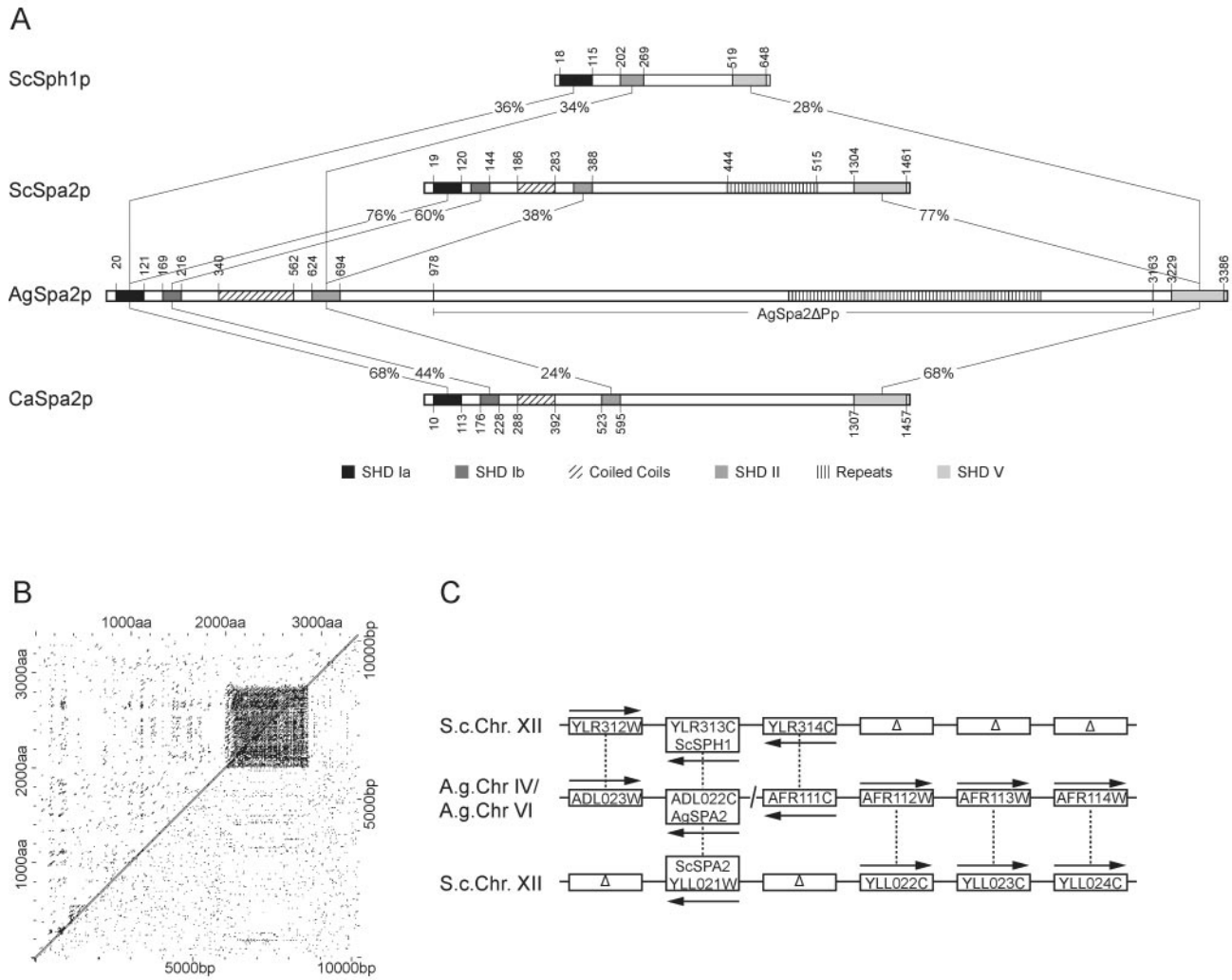

Figure 2. Analysis of AgSpa2p and its coding region. (A) Alignment of AgSpa2p, ScSpa2p, CaSpa2p, and ScSph1p. Corresponding domains show the same hatching. The domain homologies between AgSpa2p and ScSpa2p, CaSpa2p and ScSph1p, respectively, are given in percent identities. The position of the individual domains is marked in aa. The deleted region in AgSPA2ΔP is marked. In *S. cerevisiae*, ScSte11p, ScMkk1p, and ScKkk2p interact with SHD Ia (Sheu *et al*., 1998), ScPea2 with SHD II (Valtz and Herskowitz, 1996), and ScBni1p with SHD V (Fujiwara *et al*., 1998). (B) Comparison of repetitive regions in AgSpa2p and the AgSPA2 ORF. Left of the diagonal line shows a comparison of the AgSpa2p versus itself and right of the diagonal a comparison of the AgSPA2 ORF versus itself. (C) Syntenic analysis of the AgSPA2 gene. Each gene is represented as a rectangle and its orientation is indicated with an arrow.

AgSpa2p Localizes Permanently to Sites of Polarized Growth

We wanted to investigate whether AgSpa2p localizes to sites of polarized growth as seen for ScSpa2p in *S. cerevisiae* (Snyder, 1989). We therefore made a C-terminal GFP fusion to the endogenous copy of the AgSPA2 ORF in the Agleu2Δthr4Δ background strain (see MATERIALS AND METHODS; Agleu2Δthr4Δ is referred to as wild type). The radial colony growth rate, the morphology, and the pattern of the actin cytoskeleton did not differ in the AgSPA2-GFP strain compared with wild type (see below).

To determine whether AgSpa2p-GFP locates transiently or permanently to growing hyphal tips, we monitored developing mycelia by fluorescence videomicroscopy. First, we started with a unipolar germling that already had AgSpa2p-GFP localized to its tip (Movie 2; selected frames in Figure 3A). Pictures were taken over a time period of 7 h at a frequency of 0.2 min^{-1}. AgSpa2p-GFP remained localized to the original tip without delocalization. The emergence of a novel lateral branch was always preceded by a concentration of AgSpa2p-GFP at the cell cortex as shown by two examples marked by arrows in Figure 3A (frames 108–110 in Movie 2). These newly initiated branches also maintained AgSpa2p-GFP permanently at their tip. AgSpa2p-GFP was also observed transiently at sites of septation but the signal was very weak under time-lapse conditions.

Second, we followed an apical branching event in 20-h-old mycelium (Movie 3; selected frames in Figure 3B). The picture acquisition frequency was 0.5 min^{-1}, the total duration 46 min. AgSpa2p-GFP permanently localized to the single growing hyphae. Before the apical branch initiation after 22 min, the AgSpa2p-GFP–labeled organelle laterally enlarged and divided symmetrically. Two independent branches formed, which again permanently localized AgSpa2p-GFP to their tip.

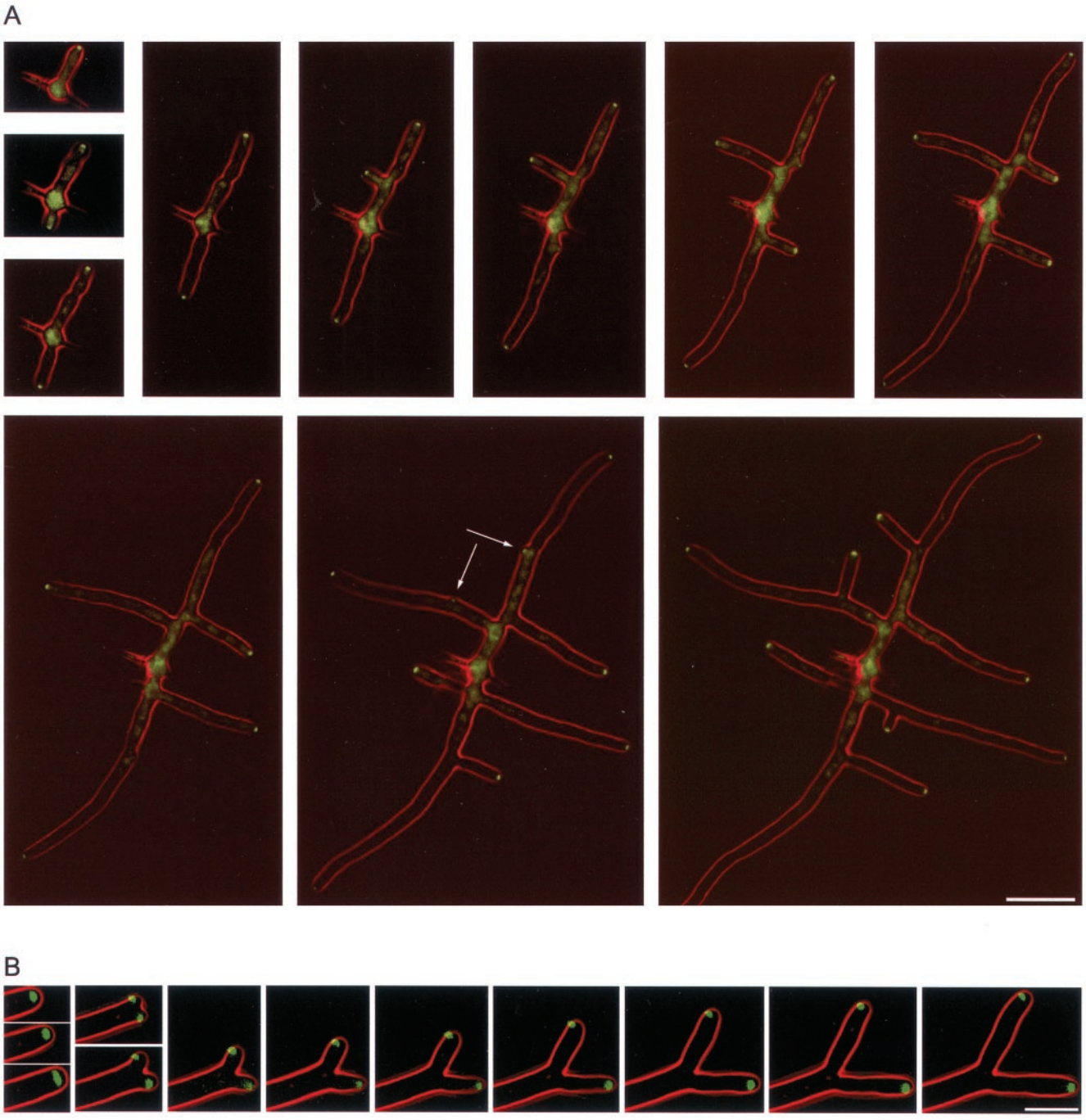

Figure 3. Temporal organization of AgSpa2p-GFP during *A. gossypii* development. The GFP signal is indicated in green, the phase contrast in red. (A) Development from a spore to a young mycelium. The time elapsed between two frames is 1 h. Localization of AgSpa2p-GFP to the hyphal cortex before lateral branch emergence is indicated with arrows. The permanent localization pattern at hyphal tips was confirmed in two additional time-lapse acquisitions. As proven in still pictures, the cytoplasmic fluorescence observed toward the image center is an artifact induced by an uneven illumination of the sample. Refer also to supplemental Movie 2. Bar, 20 μm. (B) Apical branching after 20 h of development. The time elapsed between two frames is 2 min. Between frame 3 and 9 the GFP signal seems not to localize exactly to the hyphal tip. This is an artifact induced by different focal planes of the bright-field and the fluorescence image. This is also the reason for the weak GFP signal for the lower tip in frame 6. The localization pattern of AgSpa2p-GFP during apical branching was confirmed in one additional time lapse acquisition. Refer also to supplemental Movie 3. Bar, 10 μm.

To reinvestigate the observed weak and transient localization of AgSpa2p-GFP at sites of septation, we performed a costaining with rhodamine-phalloidin. A typical example is presented in Figure 4 showing from left to right a differential interference contrast (DIC), GFP fluorescence, and rhodamine-phalloidin fluorescence image of the same young my-

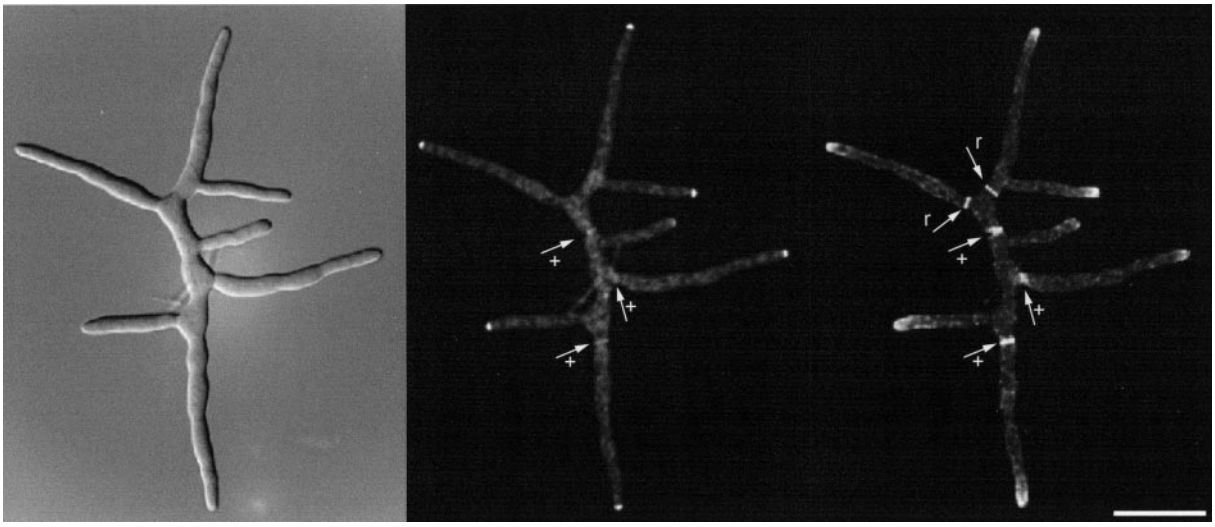

Figure 4. AgSpa2p-GFP/rhodamine-phalloidin double staining. Left, DIC; middle, AgSpa2p-GFP; and right, rhodamine-phalloidin. r, actin rings during early stages of septation and +, actin patches and AgSpa2p-GFP, respectively, at sites of septation during later developmental stages. See also Figure 1. Bar, 20 μm.

celium. All tips display AgSpa2p-GFP and actin patch staining; however, there is no complete colocalization. The GFP fluorescence is focused to the very tip, whereas the actin patches are dispersed over a wider tip region. 3D reconstruction of the actin staining could distinguish between actin rings (probably actomyosin) and actin patches at sites of ongoing septation (see arrows labeled with r representing actin rings and + representing actin patches in Figure 4, right). Only those sites containing actin patches were found to contain AgSpa2p-GFP (arrows in middle panel). AgSpa2p was not observed at sites of actin rings. Neither was it seen to colocalize with actin cables nor cortical actin patches in 10 3D reconstructions analyzed (our unpublished data).

In summary, polarization during morphogenesis in *A. gossypii* is characterized by an early appearance of AgSpa2p at emerging lateral branch sites, a permanent localization of AgSpa2p at hyphal tips including tip branching, and a transient location at sites of septum formation.

AgSpa2p Is Required for Fast Radial Colony Growth

To investigate the role of AgSpa2p in *A. gossypii* morphogenesis, we generated two mutant alleles of AgSPA2. A complete deletion of the AgSPA2 ORF was generated by PCR-based gene targeting (Wendland *et al*., 2000). We deleted the complete coding region downstream of the start codon creating the Agspa2ΔC allele. Additionally, 86% of the internal domain in AgSPA2 (codon 978-3163) was deleted, creating the AgSPA2ΔP allele. A C-terminal GFP-tagged version of this strain was also constructed (Figure 2; MATERIALS AND METHODS).

The AgSPA2ΔP and Agspa2ΔC mutant strains had a colony growth defect that was more pronounced in the complete deletion strain. When grown on AFM plates for 6 d, the radial colony growth distance of the partial deletion strain was 63% compared with the wild-type, whereas the complete deletion only 40% (Figure 5A). To determine whether this colony growth defect was the result of a decreased radial growth speed, we determined the radial growth speed of wild-type, AgSPA2ΔP, and Agspa2ΔC colonies over a time frame of 7 d. Pregrown mycelium was inoculated in the center of AFM plates. The mycelia were cultured at 30°C, and the radial diameter of the colony was measured every 24 h. All three strains reached their maximal radial colony growth speed after 3 d. For wild type, this was ~190 μm/h, for AgSPA2ΔP 120 μm/h, and for Agspa2ΔC 80 μm/h (Figure 5B). The radial colony growth speed decreased afterward for all strains. AgSPA2-GFP and AgSPA2ΔP-GFP grew indistinguishable from the respective untagged versions (Figure 5B).

AgSpa2ΔPp-GFP displayed a very similar localization pattern as the full-length protein. It was found at hyphal tips, at emerging branch sites, and at sites of septation. To rule out that the decreased radial colony growth speed observed for AgSPA2ΔP was due to an unstable localization of AgSpa2ΔPp, we compared the frequency of apical GFP localization between AgSpa2p-GFP and AgSpa2ΔPp-GFP. We found that 91% of all hyphae had the full-length protein localized to tips and 90% the partially deleted protein ($n > 80$; Figure 5C).

To exclude that the observed decrease in radial colony growth speed in Agspa2ΔC was due to a less frequent polarization of hyphal tips, we determined the frequency of polarized cortical actin in that strain and compared it with wild type. We also included the partially deleted and the two GFP fusion strains. Spores of all five strains were cultured in AFM at 30°C and fixed after 16 h (see MATERIALS AND METHODS). The mycelia were stained for actin, and polarized actin at hyphal tips was quantified. All strains displayed polarized actin at hyphal tips at a frequency of $\geq$98% ($n > 100$).

We conclude that AgSpa2p is required for fast radial colony growth and that the extended internal domain plays an important role in that process. AgSpa2p is not required to polarize cortical actin to tips.

Analysis of Hyphal Tip Morphology in AgSPA2ΔP and Agspa2ΔC

We investigated potential differences in hyphal tips with respect to organization of the actin cytoskeleton, hyphal tip diameters, and the expansion of AgSpa2p-GFP and

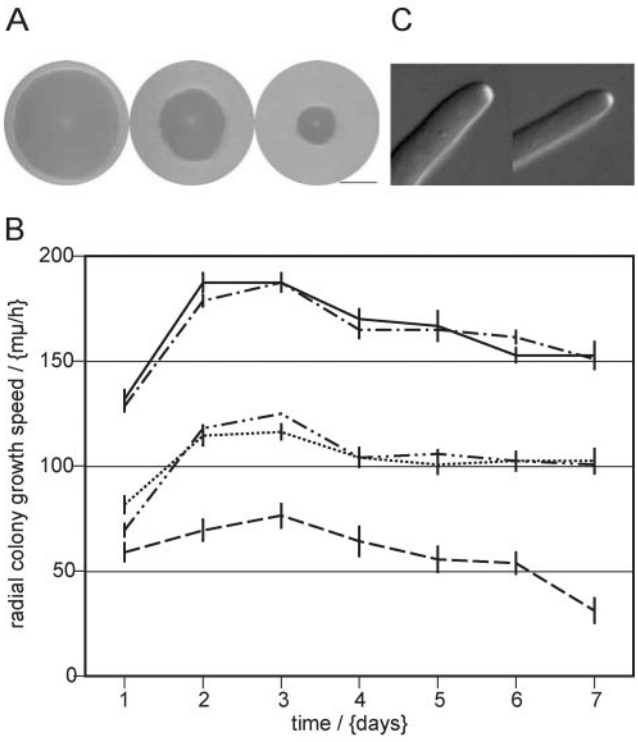

Figure 5. Radial colony growth phenotype in AgSPA2ΔP and Agspa2ΔC strains. (A) Left, wild-type; middle, AgSPA2ΔP; and right, Agspa2ΔC. All mycelia were grown for 6 d at 30°C. Bar, 2 cm. (B) Radial growth speed of wild type, AgSPA2ΔP, and Agspa2ΔC strains. The *x*-axis represents the time in days and the *y*-axis the radial growth speed in micrometers per hour (error bar, SEM). Wild type (——), AgSPA2-GFP (– – –), AgSPA2ΔP (- - -), AgSPA2ΔP-GFP (– - – -), and Agspa2Δ (– – –). The value measured after the 1st d was the difference between the inocula (1 mm in diameter) and the radial growth distance after 1 d divided by 24 h. The inocula were taken from plates that had already been growing for 3 d and should have reached the maximal radial growth speed. We suppose therefore that the value for day 1 (especially for the strains carrying the full-length and partially deleted alleles) is too low. (C) Localization of AgSpa2p-GFP (left) and AgSpa2ΔPp-GFP (right) to hyphal tips. DIC in gray and GFP in white.

AgSpa2ΔPp-GFP in hyphal tips. The organization of the actin cytoskeleton in tips of the AgSPA2ΔP and Agspa2ΔC strains, respectively, did not differ significantly from wild type. Actin patches localized to the tip and actin cables were visible at the cortex of the hyphae. Also actin rings were identified at the cortex of hyphae in subapical regions of both mutants.

The arc-like expansions of the GFP signal in the AgSPA2-GFP and the AgSPA2ΔP-GFP strain were not identical (Figure 5C). The arc end-to-end distance was 2.3 ± 0.05 μm for AgSpa2p-GFP and 1.9 ± 0.06 μm for AgSPA2ΔPp-GFP (n = 30).

To determine the area of growth at the tip, we measured the hyphal diameter. From time-lapse analysis, we showed that the hyphal diameter reflects the area of growth at the tip because the hyphal diameter remained constant in subapical regions except at emerging lateral branch sites. Therefore, the hyphal diameter was determined at tip regions of at least 25 μm in length. The diameter for wild-type tip regions is 4.2 ± 0.06 μm, for AgSPA2ΔP 3.7 ± 0.03 μm, and for Agspa2ΔC 5.8 ± 0.08 μm (SEM; n > 23 for each strain).

Together, AgSpa2p has an impact on the area of growth at the tip and the extended internal domain plays an important role in this process. The missing internal domain in AgSPA2ΔP has a direct effect on the expansion area of AgSpa2ΔPp We could not detect differences in the actin cytoskeleton concerning the actin patch and the actin ring organization, respectively. However, we cannot exclude differences in the number of tip-located actin cables in the three strains.

The Radial Colony Growth Defect Is the Consequence of a Decreased Hyphal Tip Growth and Speed

Apparently, the function of AgSpa2p at hyphal tips is important for optimal colony growth. To investigate the function of AgSpa2p in mycelial morphogenesis, wild type, AgSPA2ΔP, and Agspa2ΔC spores were analyzed during development from spores to mature mycelia in respect to morphogenesis and tip growth speed.

Spores from all three strains were allowed to germinate on slides covered with AFM (MATERIALS AND METHODS). After 8 h, individual spores that had developed to unipolar germlings were followed at a picture frequency of 0.5 h^{-1} over a time period of 16 h. To investigate later developmental stages, hyphae were also followed at the edge of 3-d-old colonies.

The general growth morphology was similar for all three strains (Figure 6A). Growth started with an initial isotropic growth phase generating a germ bubble. Next, the switch to polarized growth lead to a first germ tube forming a unipolar germling. The primary germ tube extended and subsequently a second germ tube emerged generating the bipolar germling. Then, lateral branches were initiated to form a young mycelium. In wild type and AgSPA2ΔP, the first apical branches started to shown up after 16 h of growth. In Agspa2ΔC, lateral branches started to show up at 10 h, and at 16 h each mycelium displayed on average five to six apical branches (n > 20). Septa were displayed in all strains. Hyphae at later developmental stages at the edge of 3-d-old colonies formed solely apical branches. Lateral branches might have emerged from hyphae in regions closer to the colony center but could not be identified any more. The distance between lateral branch sites and tips at leading edges of mature mycelium must thus have exceeded 150 μm in all strains.

In wild type, the hyphal tip growth speed of the main hyphae reached 92 μm/h after 16 h of growth. The maximal value observed for a single hypha was 167 μm/h. The hyphal tip growth speed determined after 3 d of growth on plates was constant at 172 μm/h during the period of measurement (Figure 6B). The hyphal tip growth speed determined for AgSPA2ΔP was decreased compared with wild type at all time points measured. The hyphal tip growth speed reached a value of 49 μm/h after 16 h of growth and a speed of 115 μm/h after 3 d of growth on plates. The initial hyphal tip growth speed (2–12 h) measured for Agspa2ΔC was increased compared with wild type. After 12 h of growth, Agspa2ΔC reached 44 μm/h, whereas wild-type reached only 33 μm/h. At 14 h, the acceleration decreased and the hyphal tip growth speed reached a value of 66 μm/h after 16 h. The hyphal tip growth speed determined for hyphae on 3-d-old plates was 80 μm/h. The discontinuous behavior of the growth speed between 10 and 14 h was most likely due to premature apical branching in this mutant.

The microscopic observations of Figure 6A clearly demonstrate differences in branching densities of the mutants

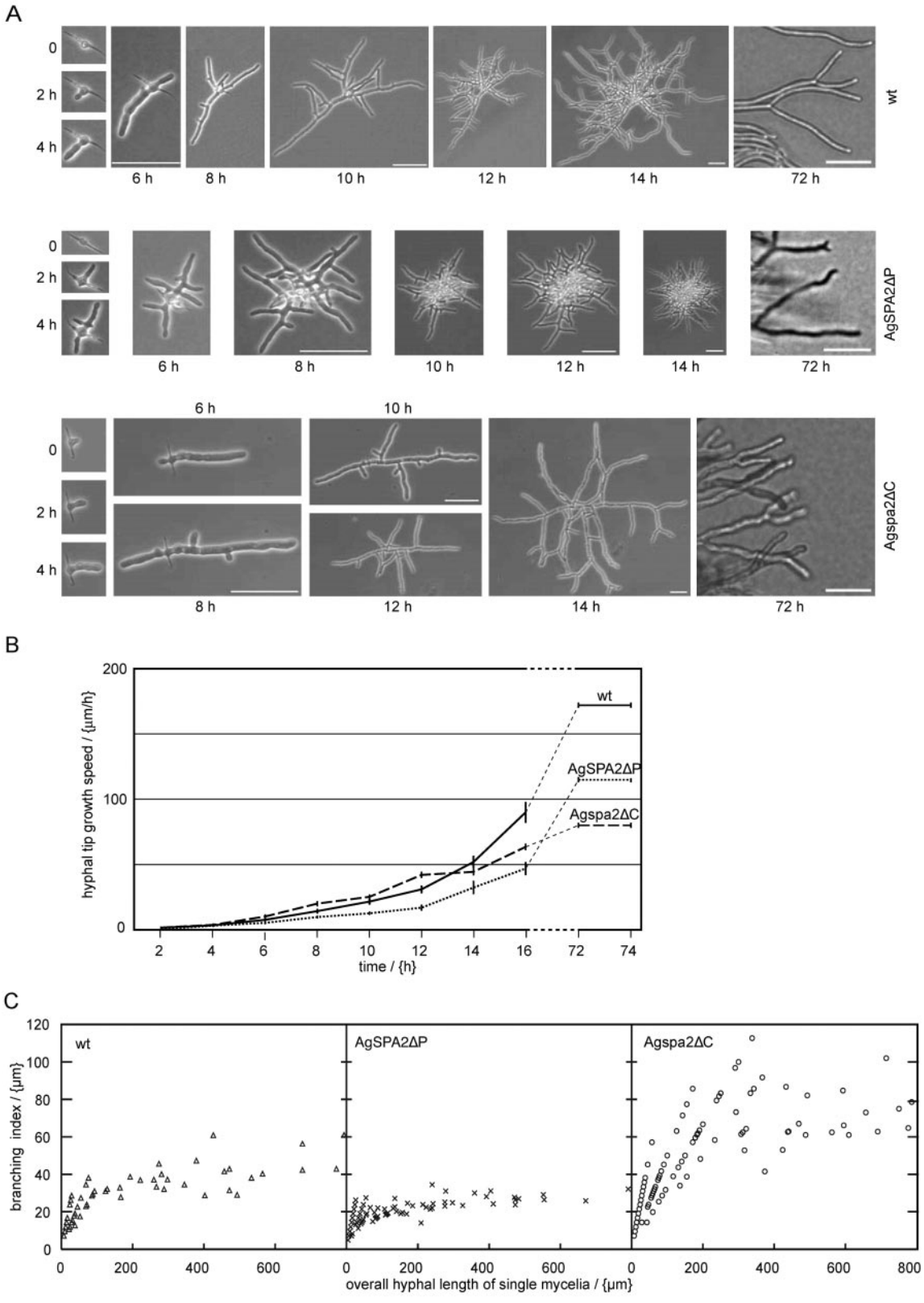

Figure 6. Quantification of development from spores to mature mycelia in wild type, AgSPA2ΔP, and Agspa2ΔC. (A) Morphological analysis. The time elapsed between two frames is 2 h, whereas the last frame corresponds to the morphological stage after 72 h. Bar, 50 μm. (B) Hyphal tip growth speed. The *x*-axis represents the time in hours and the *y*-axis the hyphal tip growth speed in micrometers per hour. Wild type (——), AgSPA2ΔP (- - -), and Agspa2ΔC (– – –) (error bar, SEM; n > 20 for each point). (C) Branching index. The *x*-axis represents the total hyphal length of single mycelia and the *y*-axis the total hyphal length of single mycelia divided by the number of tips.

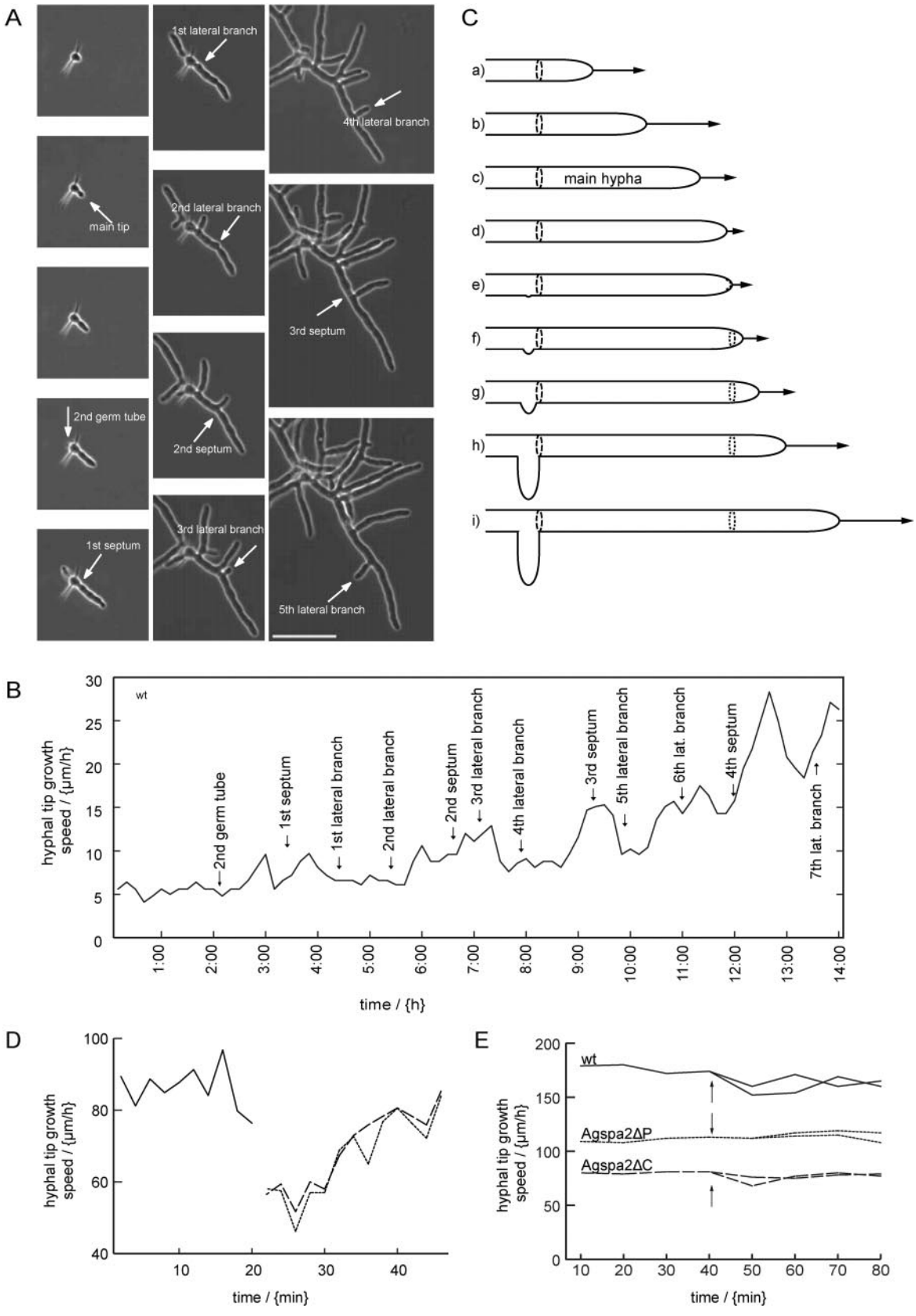
A
1st lateral branch
4th lateral branch
main tip
2nd lateral branch
3rd septum
2nd germ tube
2nd septum
3rd lateral branch
1st septum
5th lateral branch
C
a)
b)
c)
main hypha
d)
e)
f)
g)
h)
i)
B
wt
hyphal tip growth speed / {µm/h}
2nd germ tube
1st septum
1st lateral branch
2nd lateral branch
2nd septum
3rd lateral branch
4th lateral branch
3rd septum
5th lateral branch
6th lat. branch
4th septum
7th lat. branch
time / {h}
D
hyphal tip growth speed / {µm/h}
time / {min}
E
wt
Agspa2ΔP
Agspa2ΔC
hyphal tip growth speed / {µm/h}
time / {min}

Figure 7.

compared with wild type. For example, a 14-h young mycelium of AgSPA2ΔP displays on average decreased distances between two adjacent lateral branches compared with wild type. In contrast, a 14-h young mycelium of Agspa2ΔC displays increased distances between two lateral branches. A quantification of these differences is compiled in Figure 6C. Branching indices were determined by measuring the total hyphal length of single mycelia. These lengths were plotted against the length divided by the number of tips in the respective mycelia (Trinci, 1970). This so called branching index reveals the average distance between lateral branches and is constant after a certain time of development. These plots show for short hyphal distances a branching index of 45 μm for wild type, 27 μm for AgSPA2ΔP, and 72 μm for Agspa2ΔC.

Together, mutations in AgSPA2 have an effect on the hyphal tip growth speed and on the branching density. We conclude that the observed radial colony growth defect in AgSPA2ΔP and Agspa2ΔC is the direct consequence of a decreased hyphal tip growth speed in the two mutants because the hyphal tip growth speed determined at the edge of colonies corresponds well with the radial colony growth speed (Figure 5). Unexpectedly, the hyphal tip growth speed during early developmental stages in the Agspa2ΔC strain was increased compared with wild-type as well as the altered branching densities in the two AgSPA2 mutant strains. To investigate in more detail this apparent correlation between branching density and hyphal tip growth speed, we monitored the early development of mycelia at high resolution.

Branching and Septation Interrupts the Increase of the Hyphal Tip Growth Speed during Early Development at Similar Frequencies in Wild Type, AgSPA2ΔP, and Agspa2ΔC

Spores from the wild-type strain were allowed to germinate on time-lapse slides at room temperature (25°C). Pictures from a single spore were acquired at a frequency of 0.5 min^{-1} (MATERIALS AND METHODS) over a time period of 15 h. The hyphal tip growth speed of the first germ tube that emerged (the main tip) was determined every 10 min and plotted against time (Figure 7, A and B, and supplemental Movie 4).

During the observed 15 h of growth, we followed the formation of nine branches and four septa initiated in the apical compartment, i.e., not interrupted by a septum from the main tip. Each of these polarization events caused the hyphal tip growth speed of the main tip to slow down. After each polarization event the hyphal tip growth speed of the main tip increased to reach the next maximum. Initiation of branches or septa in compartments that were separated from the main tip by one or more septa did not have an effect on the hyphal tip growth speed of the main tip. The initial hyphal tip growth speed was 5 μm/h and reached 26 μm/h after 14 h of growth; Figure 7B). Spatial analysis of lateral branching and septation revealed furthermore that the site selection of these events was not random. The initiation of a lateral branch or a septum caused the hyphal tip growth speed of the main tip to decrease transiently. During this transient decrease a landmark is very likely established at the tip of the main hypha that remains at the cortex. Exclusively these sites served as potential initiation points for new septa or lateral branches. For example, the position that the main tip reached during the emergence of the second septum served as initiation point for the fourth lateral branch and the third septum, respectively (Figure 7, A and C, and supplemental Movie 4). This could also be observed for AgSPA2ΔP and Agspa2ΔP.

We conclude that lateral branching and septation are morphogenic events that interrupt the increase of the hyphal tip growth speed during the development from a spore to a young mycelium. Presumptive sites for lateral branching and septation, respectively, are previously marked at the hyphal tip in response to a precedent branching or septation event.

For AgSPA2ΔP and Agspa2ΔC the effect on the hyphal tip growth speed upon branching or septation was similar as observed in wild type (our unpublished data; experiments in duplicate). Each of these events interrupted the increase of the hyphal tip growth speed. Analysis from the frequency of interruptions of the hyphal tip growth speed did not reveal substantial differences between wild type, AgSPA2ΔP, and Agspa2ΔC. New sites of polarization were established at similar frequencies during early development in all three strains.

Figure 7 (facing page). Behavior of the hyphal tip growth speed during the development of a spore to a mature mycelium. (A) Time-lapse acquisition of wild type at 2-min intervals. The time elapsed between the frames shown is 1 h. We followed the development of the first emerging germ tube (main tip). Sites of septation and lateral branch emergence are marked by arrows. We show the emergence of five lateral branches of nine observed and three septation events of four observed. Bar, 50 μm. Refer also to supplemental Movie 4. (B) Hyphal tip growth speed of wild type at medium resolution. The basis for this graph is the supplemental Movie 4, representative frames are shown in A. The *x*-axis represents the elapsed time in min and the *y*-axis the hyphal tip growth speed in micrometers per hour. Labeled arrows mark the initiation of septa and branches. Lateral branches show up 10–20 min after a hyphal tip growth speed decrease, whereas septa seem to occur slightly later. The reason for this might be that the beginning of a septum formation cannot be seen in phase contrast microscopy. We marked the emergence of seven lateral branches and four septations. This pattern was confirmed in two additional time lapse acquisitions. (C) Presumptive landmarks for lateral branching and septation in *A. gossypii*. The illustration shows the establishment of a lateral branch at a presumptive landmark (dashed ring) during development of a young *A. gossypii* mycelium. The outline of the hypha is indicated, and the changes in hyphal tip growth speed are represented by arrows of different lengths. During early development, the hyphal tip growth speed increases (a and b). Before lateral branch formation, the hyphal tip growth speed transiently decreases (c and d) and then accelerates again (e–i). The lateral branch emerges concomitant with the reacceleration of the main hypha or with a slight delay (e). During or after the transient decrease (c and d), a landmark is established at the tip (e, dotted line) that remains at the hyphal cortex (f–i, dotted ring) and marks a future branching and/or septation site. The timing for the establishment of new lateral branches and septa, respectively, and the decision whether to form a lateral branch or a septa are so far unclear. (D) Hyphal tip growth speed during apical branching in early development (16–20 h). This graph is based on a quantitative analysis of supplemental Movie 3, representative frames of which are shown in Figure 3B. The *x*-axis represents the elapsed time in minutes and the *y*-axis the hyphal tip growth speed in micrometers per hour. Apical branching occurs after 22 min with a concomitant decrease in tip growth speed of the two new hyphae. The solid line shows the hyphal tip growth speed before apical branching and the dashed and dotted lines the hyphal tip growth speeds after apical branching. This decrease and reacceleration was confirmed in one additional time lapse acquisition. (E) Lack of significant decrease in tip growth speed during apical branching in mature mycelium (3 d). Mature hyphae were followed by time lapse acquisitions in wild type, AgSPA2ΔP, and Agspa2ΔC strains (Figure 6A). The initiation of an apical branch is indicated with arrows. The hyphal tip growth speeds of both tips resulting from the apical branch were determined. Wild type (——), AgSPA2ΔP (- - -), and Agspa2ΔC (– – –). Five independent apical branching events were observed for each strain giving similar results.

Thus, the apparent hyper- and hypobranching phenotype in the respective AgSPA2 mutant strains (Figure 6, A and C) does not necessarily represent an alteration in the temporal control of the branching frequency. We rather assume that in the case of AgSPA2ΔP and Agspa2ΔC, respectively, the differences in the branching indices during early development are the result of a constant branching and septation frequency at different hyphal tip growth speeds.

A decrease of the hyphal tip growth speed could also be observed during apical branching in young mycelium (Figure 7D). In contrast, we could not observe a substantial decrease of the hyphal tip growth speed in mature mycelium measured on 3-d-old mycelia in wild type, AgSPA2ΔP, and Agspa2ΔC. Only decreases of <10% of the average hyphal tip growth speed were observed lasting for maximal 20 min (Figure 7E, determined from 10 individual growing hyphae). Apparently, in contrast to early stages of development, branching or septation influences the hyphal tip growth speed at later developmental stages just occasionally and then weakly.

DISCUSSION

Temporal and Spatial Organization of Polarization in Filamentous Growth

Sites of polarization in *A. gossypii* are localized at hyphal tips and at sites of septum formation as judged by rhodamine-phalloidine staining. AgSpa2p localizes to these sites and thus is a marker of polarization. Polarization is established and permanently maintained upon germ tube formation and lateral branch emergence. The polarization at hyphal tips, as evident from the presence of AgSpa2p, is also maintained during decrease of the hyphal tip growth speed in response to a novel polarization event. Permanent polarization of hyphal tips in *A. gossypii* clearly differs from the transient polarization pattern observed in the budding yeast. There, polarization is established at the presumptive bud site. At the G2/M transition, growth is redirected over the entire bud cortex and subsequently polarized to the site of septation (Lew and Reed, 1995). This transient polarization at bud tips in *S. cerevisiae* is also observed during pseudohyphae formation (Pruyne and Bretscher, 2000a,b). In the dimorphic fungus *Candida albicans*, the polarization pattern is transient during the budding cycle as in *S. cerevisiae*, whereas a permanent polarization of the actin cytoskeleton can be observed during filamentation (Sevilla and Odds, 1986; Hazan *et al*., 2002).

The establishment of polarization sites does not occur randomly in *A. gossypii* but at preformed landmarks. The formation of a new lateral branch or septum causes a transient decrease of the hyphal tip growth speed. During this phase of slower tip extension, a marker is established at the hyphal tip that persists at the cortex to direct future branching or septation events. A candidate for such a marker might be the landmark protein AgBud3p (Wendland, 2003).

In the filamentous fungus *Neurospora crassa*, the statistical distribution of branch-to-branch distance seems to constitute a homeostatic set point (Watters *et al*., 2000; Watters and Griffiths, 2001) and in *Geotrichum candium* and *A. nidulans* the ratio of mycelial length to the number of branches tends toward a steady-state value (Prosser and Trinci, 1979). Rules for a branching and septation pattern, however, have not been suggested yet for filamentous fungi. In *S. cerevisiae*, rules for the budding pattern exists that have been extensively used to characterize mutants (Casamayor and Snyder, 2002). The spatial organization of polarization in *A. gossypii* remotely resembles the bipolar budding pattern of diploid *S. cerevisiae*. Yeast daughter cells bud uniquely distal to the mother/bud neck, which leads to the formation of a filament-like structure after several divisions on solid medium. Proximal or distal budding in mother cells resembles the formation of lateral branches in *A. gossypii*. Apical branching, which represents the division of an existing polarization, has not been observed in *S. cerevisiae* and represents a unique morphogenetic event in several filamentous fungi. Nothing is known about the mechanism controlling this apical branching.

Hyphal Tip Growth Speed during Mycelium Development in A. gossypii

During the development from a spore to a mycelium, the hyphal tip growth speed increases. The subapical region represents a comparably large surface for uptake of nutrients. The surface area steadily increases due to the expanding hyphal tip, which might be the reason for the increase in hyphal tip growth speed. As long as the capacity of incorporating secretory vesicles exceeds their transport to the tip, the hyphal tip growth speed can increase. When the transport to the tip is equal to or exceeds the incorporation, the hyphal tip growth speed becomes constant. Therefore, the speed of hyphal tip extension is determined by two factors, the transport of secretory vesicles to the tip and their subsequent incorporation (Katz *et al*., 1972; Trinci *et al*., 1994; Watters and Griffiths, 2001).

The increase of the hyphal tip growth speed in *A. gossypii* was abolished in response to the establishment of new branches or septa. The possibility that branching can impair the hyphal tip growth speed had been previously suggested for the filamentous ascomycetes *A. nidulans* (Trinci, 1970) and *Aspergillus oryzae* (Spohr *et al*., 1998; Christiansen *et al*., 1999). We suggest that the establishment of lateral branches and septa redirects the transport of a portion of secretory vesicles away from the main tip to the sites of branch and septum initiation, respectively. During later stages of *A. gossypii* development, when the hyphal tip growth speed reached a maximum value, this growth speed is no longer decreased upon branching or septation. The limiting factor during this later developmental stage is most likely the incorporation efficiency of vesicles at the tip and not their transport. We assume that this transport may even exceed the maximal capacity of vesicle incorporation and therefore vesicles probably accumulate at the tips in mature mycelium. This accumulation above a certain level possibly will trigger apical branching and explains at the same time why at that stage no significant decrease in tip growth speed is observed.

Oscillations of hyphal tip extension rate has been reported as pulsed growth of hyphal tips in several fungal species (Lopez-Franco *et al*., 1994, Jackson, 2001). These studies reported relatively short growth pulses of 3- to 45-s duration in mature mycelium probably reflecting the intervals of docking and fusion of secretory vesicles at the growing tip. These pulses are not coordinated with branching or septation events as described herein. It is conceivable that short pulses of growth also drive hyphal tip extension in *A. gossypii*. The observed transient decrease of the hyphal tip growth speed in *A. gossypii* mycelia, however, is strictly associated with branching or septation and occurs in intervals of ~1 h. Filamenting cells of *C. albicans* have a constant hyphal tip growth speed, also during septation (Gow and Gooday, 1982; Sevilla and Odds, 1986). The reason for this might be that the micropore in the septum is too small to allow organelle or cytoplasm exchange between adjacent compartments (Gow *et al*., 1980) and thus the hyphal tip growth is supported only from a relatively small cytoplasmic compartment.

AgSpa2p Determines the Area of Growth at the Hyphal Tip

A deletion of the complete AgSPA2 ORF caused a 53% decrease in the maximal hyphal tip growth speed. Deleting the coding region for the extended internal domain in AgSpa2p alone caused a decrease of 33%. One possible explanation for the AgSPA2ΔP phenotype might be a decrease in the expression level. However, comparisons of tip-located fluorescence intensity between AgSpa2p-GFP and AgSPA2ΔPp-GFP reveal no major differences. Because the colony growth speed of AgSPA2-GFP and AgSPA2ΔP-GFP did not differ from what was observed for the untagged strains, we conclude that the colony growth defect observed in AgSPA2ΔP is the consequence of the missing internal domain.

We suggest that the function of AgSpa2p is in the organization of incorporating secretory vesicles at the tip due to the following reasons. First, AgSpa2p localizes to sites of polarized growth. Second, different hyphal diameters observed in the two AgSPA2 mutants is the direct consequence of a function at the hyphal tip. Third, apical branching is assumed to indicate that the transport of secretory vesicles to the tip exceeds their incorporation. In mature mycelium both AgSPA2 mutant strains exhibit apical branching at similar frequencies as observed in wild type. This indicates that vesicles are present at hyphal tips in excess in the two mutant strains. However, the maximal hyphal tip growth speed is reduced in the mutant strains; though not the transport to the tip but the organization of incorporating secretory vesicles is affected in the two mutant strains. Both the hyphal diameter and the tip area occupied by the polarisome is smaller in AgSPA2ΔP compared with wild type. This strongly indicates that the internal domain influences the expansion of the polarisome. We thus suggest that a main role of the full-length AgSpa2p in the organization of incorporating secretory vesicles at the hyphal tip might be in the determination of the area of growth, i.e., the determination of the area of incorporating secretory vesicles. This would be in agreement with the finding that ScSPA2 deletion strains in *S. cerevisiae* fail to properly localize the secretion marker ScSec4p (Sheu *et al*., 1998).

To explain the increased hyphal tip growth speed in Agspa2ΔC observed during early development we consider two different models. 1) Because branching severely decreases the hyphal tip growth speed during early development, less branching events per time would result in an increased hyphal tip growth speed and vice versa. Analysis of the branching pattern (Figure 6A) is in agreement with this interpretation because shorter branch distances can be observed in AgSPA2ΔP and longer distances in Agspa2ΔC at comparable time points. 2) Longer unbranched hyphae in the Agspa2ΔC strain directly results in an enlarged area for nutrient uptake directed to the tip. This provides the tip with more secretory vesicles and thus allows faster growth during early stages of development. We favor the second model as this is also in accordance with a model that predicts an increased hyphal extension rate when the tip is supported from a larger cytoplasm Trinci *et al*., 1994.

Molecular Implication of AgSpa2p

No experimental data are presently available characterizing interaction proteins for AgSpa2p. In *S. cerevisiae*, it was shown that the polarisome components ScSpa2p and ScBud6p interact with the formin ScBni1p where ScSpa2p is important for ScBni1p localization and ScBud6p for ScBni1p activation (Evangelista *et al*., 2002; Sagot *et al*., 2002). ScBni1p is a key component for polarized growth because it controls the assembly of actin cables and thus directs secretory vesicles to sites of polarized growth. We hypothesize that in *A. gossypii* an extended internal domain between SHD II and SHD V of AgSpa2p might differently regulate the localization of AgBni1p and thus actin cable formation to assure development to maximal tip growth speed. The further analysis of the polarisome in *A. gossypii* must therefore include the formin AgBni1p.

ACKNOWLEDGMENTS

We thank Jürgen Wendland for many supporting discussions during the initial stage of this work and are grateful for Jürgen's and Amy Gladfelter's comments on the manuscript. We also thank Martin Ackermann for help in statistical analysis. This work was supported by grants from the University of Basel and the Swiss National Science Foundation Grant 31-55941.98.

REFERENCES

Altmann-Johl, R., and Philippsen, P. (1996). AgTHR4, a new selection marker for transformation of the filamentous fungus *Ashbya gossypii*, maps in a four-gene cluster that is conserved between *A. gossypii* and *Saccharomyces cerevisiae*. Mol. Gen. Genet. *250*, 69–80.

Amberg, D.C. (1998). Three-dimensional imaging of the yeast actin cytoskeleton through the budding cell cycle. Mol. Biol. Cell *9*, 3259–3262.

Amberg, D.C., Zahner, J.E., Mulholland, J.W., Pringle, J.R., and Botstein, D. (1997). Aip3p/Bud6p, a yeast actin-interacting protein that is involved in morphogenesis and the selection of bipolar budding sites. Mol. Biol. Cell *8*, 729–753.

Arkowitz, R.A., and Lowe, N. (1997). A small conserved domain in the yeast Spa2p is necessary and sufficient for its polarized localization. J. Cell Biol. *138*, 17–36.

Ayad-Durieux, Y., Knechtle, P., Goff, S., Dietrich, F., and Philippsen, P. (2000). A PAK-like protein kinase is required for maturation of young hyphae and septation in the filamentous ascomycete *Ashbya gossypii*. J. Cell Sci. *113*, 4563–4575.

Boyce, K.J., Hynes, M.J., and Andrianopoulos, A. (2001). The CDC42 homolog of the dimorphic fungus *Penicillium marneffei* is required for correct cell polarization during growth but not development. J. Bacteriol. *183*, 3447–3457.

Casamayor, A., and Snyder, M. (2002). Bud-site selection and cell polarity in budding yeast. Curr. Opin. Microbiol. *5*, 179–186.

Christiansen, T., Spohr, A.B., and Nielsen, J. (1999). On-line study of growth kinetics of single hyphae of Aspergillus oryzae in a flow-through cell. Biotechnol. Bioeng. *63*, 147–153.

Dietrich, F., Voegeli, S., Brachat, A., Lerch, A., Gates, K., Luedi, P., Gaffney, T., and Philippsen, P. (2001). Evolution of the *S. cerevisiae* genome: lessons learned from the genome analysis of the fungus *Ashbya gossypii*. XXth International Conference on Yeast Genetics and Molecular Biology, Prague, Czech Republic.

Dietrich, F.S., *et al*. (1997). The nucleotide sequence of *Saccharomyces cerevisiae* chromosome V. Nature *387*, 78–81.

Drubin, D.G., and Nelson, W.J. (1996). Origins of cell polarity. Cell *84*, 335–344.

Evangelista, M., Blundell, K., Longtine, M.S., Chow, C.J., Adames, N., Pringle, J.R., Peter, M., and Boone, C. (1997). Bni1p, a yeast formin linking cdc42p and the actin cytoskeleton during polarized morphogenesis. Science *276*, 118–122.

Evangelista, M., Pruyne, D., Amberg, D.C., Boone, C., and Bretscher, A. (2002). Formins direct Arp2/3-independent actin filament assembly to polarize cell growth in yeast. Nat. Cell Biol. *4*, 32–41.

Finger, F.P., and Novick, P. (1998). Spatial regulation of exocytosis: lessons from yeast. J. Cell Biol. *142*, 609–612.

Fujiwara, T., Tanaka, K., Mino, A., Kikyo, M., Takahashi, K., Shimizu, K., and Takai, Y. (1998). Rho1p-Bni1p-Spa2p interactions: implication in localization of Bni1p at the bud site and regulation of the actin cytoskeleton in *Saccharomyces cerevisiae*. Mol. Biol. Cell *9*, 1221–1233.

Gehrung, S., and Snyder, M. (1990). The SPA2 gene of *Saccharomyces cerevisiae* is important for pheromone-induced morphogenesis and efficient mating. J. Cell Biol. *111*, 1451–1464.

Gow, N.A., and Gooday, G.W. (1982). Growth kinetics and morphology of colonies of the filamentous form of *Candida albicans*. J. Gen. Microbiol. *128*, 2187–2194.

Gow, N.A., Gooday, G.W., Newsam, R., and Gull, K. (1980). Ultrastructure of the septum of *Candida albicans*. Curr. Microbiol. *4*, 357–359.

Guthrie, C., and Fink, G.R. (1991). Guide to yeast genetics and molecular biology. Methods Enzymol. *194*, 14–15.

Hall, A. (1998). Rho GTPases and the actin cytoskeleton. Science *279*, 509–514.

Hanahan, D. (1983). Studies on transformation of *Escherichia coli* with plasmids. J. Mol. Biol. *166*, 557–580.

Harris, S.D. (1997). The duplication cycle in *Aspergillus nidulans*. Fungal Genet. Biol. *22*, 1–12.

Harris, S.D., Hamer, L., Sharpless, K.E., and Hamer, J.E. (1997). The *Aspergillus nidulans* sepA gene encodes an FH1/2 protein involved in cytokinesis and the maintenance of cellular polarity. EMBO J. *16*, 3474–3483.

Harris, S.D., Hofmann, A.F., Tedford, H.W., and Lee, M.P. (1999). Identification and characterization of genes required for hyphal morphogenesis in the filamentous fungus *Aspergillus nidulans*. Genetics *151*, 1015–1025.

Hazan, I., Sepulveda-Becerra, M., and Liu, H. (2002). Hyphal elongation is regulated independently of cell cycle in *Candida albicans*. Mol. Biol. Cell *13*, 134–145.

Heath, B.I. (1995). Integration and regulation of hyphal tip growth. Can. J. Bot. *73*, 131–139.

Heim, R., and Tsien, R.Y. (1996). Engineering green fluorescent protein for improved brightness, longer wavelengths and fluorescence resonance energy transfer. Curr. Biol. *6*, 178–182.

Hoepfner, D., Brachat, A., and Philippsen, P. (2000). Time-lapse video microscopy analysis reveals astral microtubule detachment in the yeast spindle pole mutant cnm67. Mol. Biol. Cell *11*, 1197–1211.

Jackson, S. (2001). Do hyphae pulse as they grow? New Phytol. *151*, 556–560.

Johnson, D.I. (1999). Cdc *42*, An essential Rho-type GTPase controlling eukaryotic cell polarity. Microbiol. Mol. Biol. Rev. *63*, 54–105.

Katz, D., Goldstein, D., and Rosenberger, R.F. (1972). Model for branch initiation in *Aspergillus nidulans* based on measurements of growth parameters. J. Bacteriol. *109*, 1097–1100.

Lengeler, K.B., Davidson, R.C., D'Souza, C., Harashima, T., Shen, W.C., Wang, P., Pan, X., Waugh, M., and Heitman, J. (2000). Signal transduction cascades regulating fungal development and virulence. Microbiol. Mol. Biol. Rev. *64*, 746–785.

Lew, D.J., and Reed, S.I. (1993). Morphogenesis in the yeast cell cycle: regulation by Cdc28 and cyclins. J. Cell Biol. *120*, 1305–1320.

Lew, D.J., and Reed, S.I. (1995). Cell cycle control of morphogenesis in budding yeast. Curr. Opin. Genet. Dev. *5*, 17–23.

Lopez-Franco, R., Bartnicki-Garcia, S., and Bracker, C.E. (1994). Pulsed growth of fungal hyphal tips. Proc. Natl. Acad. Sci. USA *91*, 12228–12232.

Maizel, J.V., Jr., and Lenk, R.P. (1981). Enhanced graphic matrix analysis of nucleic acid and protein sequences. Proc. Natl. Acad. Sci. USA *78*, 7665–7669.

Momany, M. (2002). Polarity in filamentous fungi: establishment, maintenance and new axes. Curr. Opin. Microbiol. *5*, 580–585.

Momany, M., and Hamer, J.E. (1997). Relationship of actin, microtubules, and cross wall synthesis during septation in *Aspergillus nidulans*. Cell Motil. Cytoskeleton *38*, 373–384.

Momany, M., and Taylor, I. (2000). Landmarks in the early duplication cycles of *Aspergillus fumigatus* and *Aspergillus nidulans*: polarity, germ tube emergence and septation. Microbiology *146*, 3279–3284.

Momany, M., Westfall, P.J., and Abramowsky, G. (1999). Aspergillus nidulans swo mutants show defects in polarity establishment, polarity maintenance and hyphal morphogenesis. Genetics *151*, 557–567.

Prosser, J.I., and Trinci, A.P.J. (1979). A model for hyphal growth and branching. J. Gen. Microbiol. *111*, 153–164.

Pruyne, D., and Bretscher, A. (2000a). Polarization of cell growth in yeast. J. Cell Sci. *113*, 365–375.

Pruyne, D., and Bretscher, A. (2000b). Polarization of cell growth in yeast. J. Cell Sci. *113*, 571–585.

Roemer, T., Vallier, L., Sheu, Y.J., and Snyder, M. (1998). The Spa2-related protein, Sph1p, is important for polarized growth in yeast. J. Cell Sci. *111*, 479–494.

Sagot, I., Klee, S.K., and Pellman, D. (2002). Yeast formins regulate cell polarity by controlling the assembly of actin cables. Nat. Cell Biol. *4*, 42–50.

Sambrook, J., Russell, D.W., and Sambrook, J. (2001). Molecular Cloning: A Laboratory Manual, Cold Spring Harbor, NY: Cold Spring Harbor Laboratory.

Schiestl, R.H., and Gietz, R.D. (1989). High efficiency transformation of intact yeast cells using single stranded nucleic acids as a carrier. Curr. Genet. *16*, 339–346.

Schirmaier, F., and Philippsen, P. (1984). Identification of two genes coding for the translation elongation factor EF-1 alpha of *S. cerevisiae*. EMBO J. *3*, 3311–3315.

Sevilla, M.J., and Odds, F.C. (1986). Development of *Candida albicans* hyphae in different growth media–variations in growth rates, cell dimensions and timing of morphogenetic events. J. Gen. Microbiol. *132*, 3083–3088.

Sharpless, K.E., and Harris, S.D. (2002). Functional characterization and localization of the *Aspergillus nidulans* formin SEPA. Mol. Biol. Cell *13*, 469–479.

Sheu, Y.J., Santos, B., Fortin, N., Costigan, C., and Snyder, M. (1998). Spa2p interacts with cell polarity proteins and signaling components involved in yeast cell morphogenesis. Mol. Cell. Biol. *18*, 4053–4069.

Short, J.M., Fernandez, J.M., Sorge, J.A., and Huse, W.D. (1988). Lambda ZAP: a bacteriophage lambda expression vector with in vivo excision properties. Nucleic Acids Res. *16*, 7583–7600.

Snyder, M. (1989). The SPA2 protein of yeast localizes to sites of cell growth. J. Cell Biol. *108*, 1419–1429.

Snyder, M., Gehrung, S., and Page, B.D. (1991). Studies concerning the temporal and genetic control of cell polarity in *Saccharomyces cerevisiae*. J. Cell Biol. *114*, 515–532.

Spohr, A., Dam-Mikkelsen, C., Carlsen, M., Nielsen, J., and Villadsen, J. (1998). On-line study of fungal morphology during submerged growth in a small flow-through cell. Biotechnol. Bioeng. *58*, 541–553.

Steiner, S., Wendland, J., Wright, M.C., and Philippsen, P. (1995). Homologous recombination as the main mechanism for DNA integration and cause of rearrangements in the filamentous ascomycete *Ashbya gossypii*. Genetics *140*, 973–987.

Steinert, P.M., and Roop, D.R. (1988). Molecular and cellular biology of intermediate filaments. Annu. Rev. Biochem. *57*, 593–625.

Thompson, J.D., Higgins, D.G., and Gibson, T.J. (1994). CLUSTAL W: improving the sensitivity of progressive multiple sequence alignment through sequence weighting, position-specific gap penalties and weight matrix choice. Nucleic Acids Res. *22*, 4673–4680.

Trinci, A.P.J. (1970). Kinetics of apical and lateral branching in *Aspergillus nidulans* and *Geotrichum lactis*. Trans. Br. Mycol. Soc. *55*, 17–28.

Trinci, A.P.J., Wiebe, M.G., and Robson, G.D. (1994). The mycelium as an integrated entity. In: The Mycota, vol. I, ed. J.G.H. Wessels and H. Meinhardt, Heidelberg, Germany: Springer-Verlag, 175–193.

Valtz, N., and Herskowitz, I. (1996). Pea2 protein of yeast is localized to sites of polarized growth and is required for efficient mating and bipolar budding. J. Cell Biol. *135*, 725–739.

van Drogen, F., and Peter, M. (2002). Spa2p functions as a scaffold-like protein to recruit the Mpk1p MAP kinase module to sites of polarized growth. Curr. Biol. *12*, 1698–1703.

Wach, A., Brachat, A., Alberti-Segui, C., Rebischung, C., and Philippsen, P. (1997). Heterologous HIS3 marker and GFP reporter modules for PCR-targeting in *Saccharomyces cerevisiae*. Yeast *13*, 1065–1075.

Wach, A., Brachat, A., Pohlmann, R., and Philippsen, P. (1994). New heterologous modules for classical or PCR-based gene disruptions in *Saccharomyces cerevisiae*. Yeast *10*, 1793–1808.

Watters, M.K., and Griffiths, A.J. (2001). Tests of a cellular model for constant branch distribution in the filamentous fungus *Neurospora crassa*. Appl. Environ. Microbiol. *67*, 1788–1792.

Watters, M.K., Humphries, C., De Vries, I., and Griffiths, A.J. (2000). A homeostatic set point for branching in *Neurospora crassa*. Mycol. Res. *104*, 557–563.

Weiner, O.D. (2002). Regulation of cell polarity during eukaryotic chemotaxis: the chemotactic compass. Curr. Opin. Cell Biol. *14*, 196–202.

Wendland, J. (2001). Comparison of morphogenetic networks of filamentous fungi and yeast. Fungal Genet. Biol. *34*, 63–82.

Wendland, J. (2003). Analysis of the landmark protein Bud3 of *Ashbya gossypii* reveals a novel role in septum construction. EMBO Rep. *4*, 200–204.

Wendland, J., Ayad-Durieux, Y., Knechtle, P., Rebischung, C., and Philippsen, P. (2000). PCR-based gene targeting in the filamentous fungus *Ashbya gossypii*. Gene *242*, 381–391.

Wendland, J., and Philippsen, P. (2000). Determination of cell polarity in germinated spores and hyphal tips of the filamentous ascomycete *Ashbya gossypii* requires a rhoGAP homolog. J. Cell Sci. *113*, 1611–1621.

Wendland, J., and Philippsen, P. (2001). Cell polarity and hyphal morphogenesis are controlled by multiple rho-protein modules in the filamentous ascomycete *Ashbya gossypii*. Genetics *157*, 601–610.

Yanisch-Perron, C., Vieira, J., and Messing, J. (1985). Improved M13 phage cloning vectors and host strains: nucleotide sequences of the M13mp18 and pUC19 vectors. Gene *33*, 103–119.